RSC Advances




ROYAL SOCIETY OF CHEMISTRY

www.rsc.org/advances

# Biogenic nano-particulate iron-sulfide produced through sulfate and Fe(III)-(hydr)oxide reductions was enhanced by pyruvate as the electron donor

Chen Zhou[1]*, Zhuolin Liu[1], Pat Pataranutaporn[1], Raveender Vannela[1], Kim F. Hayes[2], and Bruce E. Rittmann[1]

[1] Swette Center for Environmental Biotechnology, Biodesign Institute, Arizona State University, USA

[2] Department of Civil and Environmental Engineering, University of Michigan, USA

*Corresponding author

Present address: Swette Center for Environmental Biotechnology, Biodesign Institute, Arizona State University, Tempe, AZ 85207-5701, USA

Tel: +01-480-634-3755

Email: zhou_SCEB@asu.edu

## Graphical Abstract

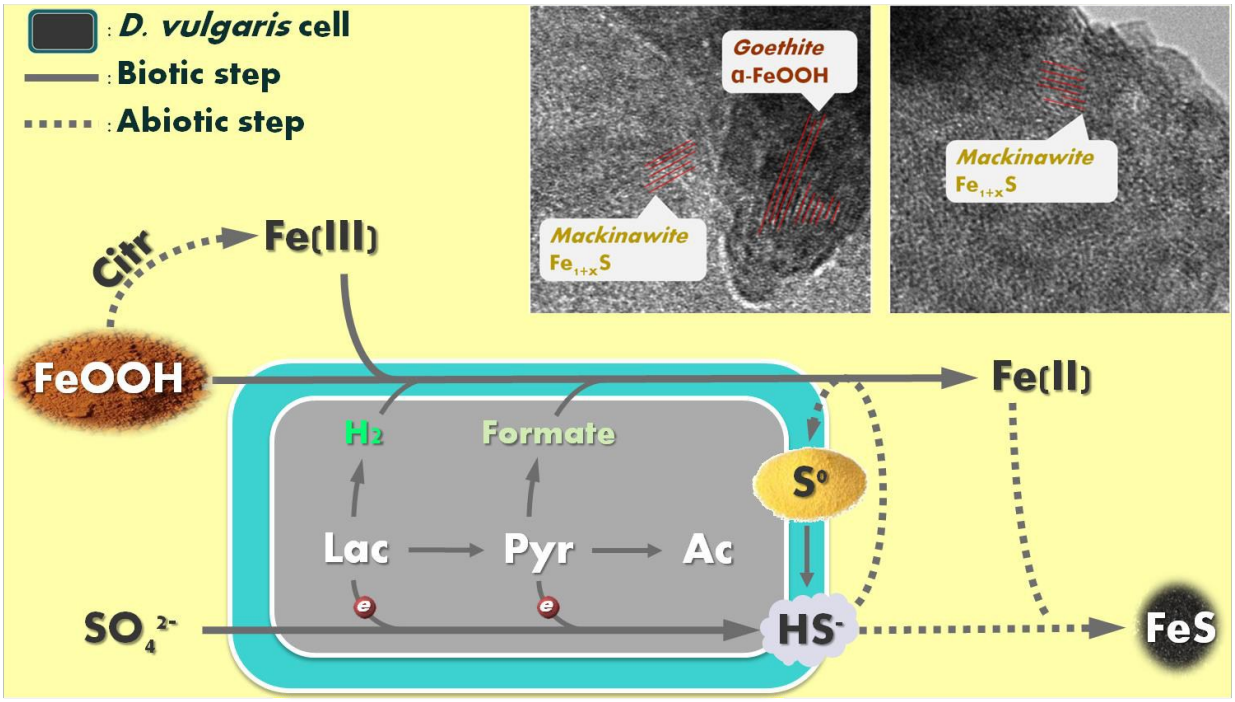

**Abstract**

In nature, formation of iron sulfide solids is mainly attributed to reductions of sulfate and ferric minerals by microorganisms such as *Desulfovibrio vulgaris*. In order to evaluate the impacts on microbial activity and optimize iron sulfide production for potential application in uranium remediation, we tested two types of electron donors (lactate and pyruvate) with three synthetic Fe(III) (hydr)oxides (goethite, hematite, and 2-line ferrihydrite). We monitored bacterial metabolism comprehensively, and we characterized the biogenic solids using transmission electron microscope equipped with energy-dispersive X-ray spectroscopy (TEM/EDX), X-ray photoelectron spectroscopy (XPS), X-ray diffraction (XRD), Raman spectroscopy, and mass distribution modeling. Despite of similarly amorphous FeS production when both $e^-$ donors were overdosed, *D. vulgaris* exhibited distinct patterns of metabolism and other solid production with the two electron donors. Once sulfate reduction was complete, further lactate fermentation was inhibited by accumulation of $H_2$, and thus limited FeS production. In contrast, *D. vulgaris* utilized all pyruvate by diverting electrons from $H_2$ to formate. In addition, the pH decrease due to the proton release during pyruvate utilization facilitated citrate-induced Fe(III) dissolution and consequently enhanced Fe(III) bioavailability. However, higher pH during lactate utilization and excess soluble Fe(II) during pyruvate utilization led to precipitation of $Ca_3(PO_4)_2$ and $Fe_3(PO_4)_2$, respectively. Together, these phenomena resulted in a substantial enhancement of Fe(III)-(hydr)oxide reduction and iron sulfide productivity with pyruvate, though the concentrations of calcium and phosphate need to be controlled to avoid precipitation of other minerals.

**Key Words:**

*Desulfovibrio vulgaris*; Fe(III) (hydr)oxide; iron sulfide; lactate; pyruvate; electron carrier.

## 1. Introduction

Iron sulfides are naturally occurring minerals derived from either biological processes or hydrothermal activity [1]. They can have various degrees of crystallinity and particle sizes, including small nano-crystallites of poorly ordered FeS, larger crystals of mackinawite, and bulk structure of greigite ($Fe_3S_4$) or pyrite ($FeS_2$, or iron polysulfide) [2-4]. Research has revealed that iron sulfides are capable of reducing soluble uranyl ion ($UO_2^{2+}$) to insoluble uraninite ($UO_2$) solids [5, 6], as well as preventing $UO_2$ from being reoxidized by $O_2$ [7, 8]. This application of iron sulfide nanoparticles has increasingly drawn attention for long-term uranium remediation [7, 9, 10]. Biogenic iron sulfide, with its nanocrystallite nature, is regarded of high redox activity due to the high specific surface area and high surface energy [6]; under this scenario, microbial-driven production of iron sulfide could potentially be an effective, economic and sustainable approach for in long-term *in situ* uranium remediation of contaminated groundwater and sediments.

The source of the sulfide for biogenic iron sulfides typically is sulfate reduction by sulfate-reducing bacteria (SRB). Our previous laboratory-based study [11] demonstrated successful production of biogenic iron sulfide nanoparticles through sulfate reduction by *D. vulgaris* and subsequent precipitation with soluble $Fe^{2+}$ as the terminal iron source. In nature, to the contrary, the $Fe^{2+}$ usually comes from bio-reduction of ferric irons carried out by iron-reducing bacteria, including some groups of SRB such as *Desulfovibrio* spp [12, 13]. Microbial Fe(III) reduction, especially of Fe(III) (hydr)oxide solids, such as goethite (α-FeOOH), hematite ($\alpha$-$Fe_2O_3$), and ferrihydrite ($Fe_2O_3$ $0.5H_2O$), significantly influences the availability of Fe(II) for the subsequent formation of FeS and may affect the characteristics of the FeS formed [14, 15].

Bio-reduction of Fe(III)-(hydr)oxides can occur by two mechanisms [16]: direct enzymatic reductions by electrons derived from electron donors (Eqns 1 – 3) and indirect chemical reductions by biogenic sulfide (Eqns 4 – 6):

$$\alpha\text{-FeOOH} + 3H^+ + e^- \rightarrow Fe^{2+} + 2H_2O \quad (1)$$

$$\alpha\text{-}Fe_2O_3 + 6H^+ + 2e^- \rightarrow 2Fe^{2+} + 3H_2O \quad (2)$$

$$Fe_2O_3\ 0.5H_2O + 6H^+ + 2e^- \rightarrow 2Fe^{2+} + 3.5H_2O \quad (3)$$

$$\alpha\text{-FeOOH} + 0.5HS^- + 2.5H^+ \rightarrow Fe^{2+} + 0.5S^0 + 2H_2O \quad (4)$$

$$\alpha\text{-}Fe_2O_3 + HS^- + 5H^+ \rightarrow 2Fe^{2+} + S^0 + 3H_2O \quad (5)$$

$$Fe_2O_3\ 0.5H_2O + HS^- + 5H^+ \rightarrow 2Fe^{2+} + S^0 + 3.5H_2O \quad (6)$$

The mechanisms and kinetics of enzymatic and chemical reductions of Fe(III) (hydr)oxides have been well studied. For enzymatic reductions, four possible mechanisms (direct contact, formation of electron shuttles, nanowires, and formation of soluble complex ligands) can explain how electrons transfer from the microbes to the solid surface [12, 17-19]. For chemical reductions by dissolved sulfide, an FeS- complex on the solid surface is rapidly formed prior to Fe(III) reduction coupled to sulfide oxidation, and the subsequent dissolution / detachment of Fe(II) has been identified as the rate-limiting step [20-22].

Previous research provides some information on the concurrent reductions of sulfate and Fe(III) by SRB, as well as the solid products. Sani, et al.[15] demonstrated distinguishable patterns of Fe(III)-(hydr)oxide reduction by *Desulfovibrio desulfuricans* G-20 for lactate-limiting versus sulfate-limiting conditions. Li et al. [23] reported only limited Fe(III) (hydr)oxide reductions by abiotic sulfide alone (5% of total iron for hematite and goethite) or enzymatically alone (less than 6% for all), but enhanced bio-reductions concomitant with abiotic reductions by biogenic sulfide from sulfate reduction by *Desulfovibrio desulfuricans* G-20 strain (64% for hematite, 74% for

goethite, and nearly 100% for ferrihydrite). Herbert et al. [24] and Gramp et al. [25] found that the predominant biogenic FeS by SRB was mackinawite under most conditions, and its crystallinity was strongly affected by environmental conditions such as temperature, time course, and Fe:S ratio. However, little is known about the impacts of different electron donors on the bacteria activities, reduction and solid-production patterns, and the mechanisms behind the phenomena. Gaining understanding of these phenomena will be of especially high value for well-studied *Desulfovibrio* species, which feature diverse patterns of intracellular electron flow with different electron donors.

The pathways for lactate and pyruvate oxidations coupled with sulfate and Fe(III) reductions are well defined for *Desulfovibrio* species [26-30]. When the starting donor is lactate ($CH_3CHOHCOO^-$), it is first partially oxidized to pyruvate ($CH_3COCOO^-$) in the periplasm, releasing protons and electrons. Pyruvate is then partially oxidized to acetate ($CH_3COO^-$) and $CO_2$, also releasing protons and electrons. These electrons can be used directly for sulfate reduction via respiration, but they also can react with membrane-bound hydrogenases to form molecular hydrogen ($H_2$) via fermentation when sulfate is absent. In addition, formate ($CHOO^-$) can be an alternative to $H_2$ as the fermentation product and electron carrier for periplasmic or extracellular reductions of other substrates, including Fe(III) (hydr)oxide solids.

Despite good knowledge of donor and acceptor catabolism in *D. vulgaris*, questions remain concerning the formation of biogenic FeS: 1) Does supplying a different electron donor (e.g., lactate versus pyruvate) directly lead to different fermentative/oxidative patterns and consequently different patterns for sulfate and iron reductions? 2) Does the type of electron donor affect other culture characteristics and microbial activities indirectly? 3) Do the overall differences affect the chemical or physical characteristics of FeS solids that form? These are the questions we address here by our systematic study of the effects of electron donor (lactate versus pyruvate) and Fe(III)

(hydr)oxide electron acceptor on the metabolism of *D. vulgaris* and the consequent formation of FeS solids. Our study documents the correlation between the biogenic iron sulfide quality and the electron donor chosen for biostimulation, fills critic gaps of the underlying mechanisms, and thus provides a baseline for the potential application of controllable biogenic FeS in U bioremediations.

## 2. Experimental

### 2.1. Strain, growth medium, and culturing conditions

*Desulfovibrio vulgaris* subsp. *vulgaris* Postgate and Campbell was purchased from the American Type Culture Collection (ATCC #29579) and grown in 160-ml serum bottles with 100 ml ATCC 1249 medium featuring key species of (in mM) lactate 31.2, sulfate 31.0, citrate 19.4, Fe(II) 3.5, Mg 16.6, Ca 7.3, and 2.9 phosphate. Details of the medium recipe and inoculation/transferring protocol are described in Zhou et al [11].

### 2.2. Iron sources

We synthesized three Fe(III)-(hydr)oxide mineral sources -- goethite (α-FeOOH), hematite (α-$Fe_2O_3$), and 2-line ferrihydrite ($Fe_2O_3$ $0.5H_2O$; ferrihydrite for short) -- as described by Schwertmann and Cornell [31]. Figure S1 presents and interprets transmission electron microscope (TEM) images of these three nanoparticulates.

### 2.3. Medium modification

In all experiments, we modified ATCC 1249 medium by 1) omitting yeast extract; 2) decreasing the sulfate concentration to ~7.5 mM by replacing $MgSO_4$ with $MgCl_2$, and 3) replacing ferrous ammonium sulfate with a target iron source at the same molar concentration as sulfate. For all experiments, we provided lactate or pyruvate at a concentration greater than the electron equivalency needed for complete reductions of sulfate and Fe(III).

We deoxygenated each modified medium by bubbling $N_2$ gas and then distributed the medium into two sterile 240-ml serum bottles (160 ml per bottle) as duplicates in an anaerobic glove box. The bottles were sealed with rubber stoppers and aluminum caps with a headspace of $N_2$ gas, and

then they were autoclaved for 15 minutes at 121°C. All iron sources other than $FeCl_2$ were added with other components at the beginning. The inocula were from fresh three-day batch cultures, with a dense biomass of 150-200 mg/l (in protein), determined by a UV–Visible spectrophotometer with Coomassie (Bradford) reagents. An initial protein concentration of ~5±1 mg/l for all experiments was obtained by injecting 3 ml of the inoculum into each bottle. The inoculated bottles were then transferred immediately to the shaker (200 rpm) and incubated at 30°C.

### 2.4. Analytical methods

For routine analyses, we transferred the experimental bottles to the anaerobic glove box and collected 3-ml liquid samples using a sterile syringe. The pH was measured first with an Epoxy Semi-Micro Combination pH Electrode (Beckman Coulter BKA57187) and a pH Meter (Beckman Coulter BKA58734). Samples were then filtered through 0.20-µm membrane filters (Whatman Inc., Haverhill, MA) for other analyses. Concentrations of soluble Fe(III) and total soluble Fe [i.e., soluble Fe(II) + soluble Fe(III)] were analyzed by the colorimetric 5-sulfosalicylic acid (SSA) method [32] using a UV–Visible spectrophotometer (Cary 50 Bio, Varian, Inc., Santa Clara, CA) at the wavelengths of 500 nm and 400 nm, respectively. Concentration of soluble Fe(II) was then calculated by subtracting soluble Fe(III) from total soluble Fe. The methods of measuring anions (including sulfate and phosphate) by ion exchange chromatography (IC) and volatile fatty acids (acetate, lactate, pyruvate, formate, and citrate) by high performance liquid chromatography (HPLC) are described in Zhou et al.[11].

We also measured soluble sulfide in the liquid phase, iron and elemental sulfur in the solid phase at the end of biotic goethite and hematite tests, as well as routinely during the biotic ferrihydrite test and the all abiotic tests. We analyzed the soluble sulfide using EPA Method 3762. We extracted all iron from the unfiltered samples (immediately after vigorous vortex) using 3%

hydrochloric acid (HCl) for 24 hours and the measured the iron dissolved in HCl (representing total iron in the original sample) using the iron TNTplus kit (Hach, Loveland, CO). Concentration of total insoluble iron was then calculated by subtracting total soluble iron from total iron. Particularly for quantifying the colloidal Fe solids in the abiotic test, we first settled the bottles on the bench for 5 minutes to exclude the rapidly-precipitating aggregates and then extracted iron from the supernatant only; the turbidly colored supernatant revealed the existence of colloidal Fe(III). We extracted elemental sulfur from the liquid samples using tetrachloroethylene for 24 hours and analyzed the dissolved sulfur using ultra performance liquid chromatography (Waters, Milford, MA, USA) with an ACQUITY UPLC column of 2.1 × 50 mm, 1.7 μm BEH $C_{18}$ [33] and an eluent of 95:5% methanol:water [34].

We also measured $H_2$ by collecting 100-μL headspace sample from each bottle with a 500 μL gas-tight syringe (Hamilton Company, Reno, NV), and injecting the gaseous sample into a gas chromatograph (Shimadzu GC-2010) equipped with a thermal conductivity detector (TCD). The standard deviation of the measurements for the $H_2$ pressure was 0.008 atm (0.3 mM), and the detection limit was 0.02 atm (1.0 mM).

### 2.5. Separation of solids from culture medium

After observing complete lactate consumption and a constant soluble Fe concentration, we placed the serum bottles in the anaerobic glove box for separation and subsequent freeze drying of the solids. The detailed procedures are described in Zhou et al. [11]. The dry and powdered solids in the serum bottles under anoxic conditions were preserved at -20°C for further analyses by transmission electron microscope equipped with energy-dispersive X-ray spectroscopy (TEM/EDX), X-ray photoelectron spectroscopy (XPS), X-ray diffraction (XRD), and Raman spectroscopy.

### 2.6. TEM/EDX analysis

Each powdered sample was loaded on a Lacey carbon 300-mesh copper TEM grid (Ted-Pella, Inc., Redding, CA, USA). TEM images were captured using a Philips CM200-FEG high resolution TEM/STEM (FEI Corp., Eindhoven, The Netherlands) operated at 200 kV, and elemental compositions at selected areas were identified using an EDX detector (EDAX Inc., Mahwah, NJ, USA).

### 2.7. XPS analysis

We performed XPS on a Vacuum Generators ESCALAB 220i-XL (Thermofisher, USA) with a monochromatic Al Kα source ($h\nu$ = 1486.6 eV, line width = 0.7 eV for Ag 3d 5/2) at a base pressure of $7 \times 10^{-10}$ mbar. To minimize the surface oxidation of FeS by oxygen in the atmosphere, the dried solids were sealed in the anoxic serum bottle with a rubber stopper before being transported from the glove box, rapidly wrapped up in the XPS room, and loaded to the XPS sample chamber for analysis under vacuum. We deconvoluted spectra with CasaXPS software.

### 2.8. XRD analysis

We performed XRD using a Rigaku D/Max-IIB diffractometer with monochromated Cu $K_\alpha$ radiation. The instrument information, analysis procedure, and calculation of average mackinawite crystallite thicknesses were described in Zhou, et al.[11]. We used the crystallite thickness data to compare the mackinawite size by assuming that 1) the mackinawite crystallite was stoichiometric tetragonal FeS, and 2) polycrystalline particles and microstrain broadening were negligible [35, 36].

### 2.9. Raman analysis

We used a thermo scientific DXR Raman spectrometer fitted with a 532 nm laser for collecting the Raman spectra. The laser power was limited to 5 mW to reduce fast oxidation and damage to these iron-containing solid samples.

### 2.10. Mass-distribution calculations

Mass balances on S and Fe were developed on the basis of eqns. 1 – 6 and by assuming that sulfate was reduced completely to sulfide by *D. vulgaris* and that iron precipitated with S was FeS. This leads to the following mass balances on $Fe^{2+}$ (Eqn. 8), total sulfur (Eqn. 9), and sulfide-S (Eqn. 10).

$$C_{\text{Fe(III) (hydr)oxide, total}} = \left[\text{Fe}^{2+}\right] + C_{\text{FeS}} + C_{\text{Fe(III) (hydr)oxide, remaining}} + C_{\text{Fe}_3(\text{PO}_4)_2\cdot 8\text{H}_2\text{O}\ (\textit{vivianite})} \quad (8)$$

$$C_{\text{S, total}} = \left[\text{SO}_4^{2-}\right]_{\text{initial}} = \left[\text{SO}_4^{2-}\right]_{\text{final}} + C_{\text{S}^{2-}\text{, total}} + C_{\text{S}^0} \quad (9)$$

$$C_{\text{S}^{2-}\text{, total}} = C_{\text{S}^{2-}\text{, free}} + C_{\text{FeS}} \quad (10)$$

Supplemental information (SI) describes the step-by-step procedure for computing the distribution of Fe and S species by combining mass-balance Eqns. 10 – 12 with mass-action equilibrium for reactions in eqns. S1 – S8.

## 3. Results and discussion

### 3.1. Formate versus $H_2$ as the $e^-$ carrier for Fe(III) (hydr)oxide reduction

Figures 1 and 2 show the patterns of bacterial growth and substrate utilization by *D. vulgaris* when the electron donor was lactate or pyruvate, respectively, and Table 1 summarizes the environmental conditions measured during incubation. In lactate-stimulated bottles, lactate consumption and corresponding acetate accumulation occurred in parallel with sulfate reduction, and they halted once sulfate was completely reduced (Fig. 1). Consequently, a significant portion of lactate remained in the end. Sulfate reduction rapidly scavenged electrons produced during lactate oxidation; however, in the absence of sulfate, $H_2$ produced during lactate fermentation began to accumulate. Previous studies with *D. vulgaris* revealed that even a small partial pressure of $H_2$ in the headspace (as low as 0.003-0.015 atm) completely inhibited further fermentation by preventing the membrane-bound hydrogenase from re-oxidizing a quinone electron carrier [29, 37-39], unless the presence of syntrophic $H_2$ consumers (e.g., methanogens) to relieve the inhibition by making the fermentation conditions energetically favorable [40, 41]. This type of $H_2$-based inhibition occurs commonly during fatty acid fermentations by many bacteria, including other *Desulfovibrio* spp. [42, 43]. In our experiments, Fe(III) (hydr)oxide reductions were not able to scavenge $H_2$ rapidly; as a result, *D. vulgaris* halted its utilization of lactate upon an accumulation of $H_2$, less than 0.02 atm according to the GC detection limit, which corresponds to only 3.4% $e^-$ equivalent from consumed lactate after complete sulfate reduction. On the other hand, formate accumulated until sulfate reduction was complete and then was consumed over 1-2 days (Fig. 1). The maximum accumulating formate accounted for less than 12% of the $e^-$ equivalents from consumed lactate in all three bottles. This indicates that, during lactate fermentation in the absence of sulfate, *D.*

197 *vulgaris* produced $H_2$ as the primary electron carrier, but also diverted a small portion of electrons
198 to formate.

199
200 In contrast to the results with lactate, *D. vulgaris* rapidly consumed all pyruvate before sulfate
201 reduction was completed (Fig. 2), resulting in more acetate accumulation than in the lactate-
202 simulated bottles. The maximum formate concentrations were much higher than in lactate-
203 stimulated bottles, especially in the hematite bottles (H-P; almost 100% of the $e^-$ equivalents from
204 consumed pyruvate went to formate) and the ferrihydrite bottles (F-P; 64% to formate). In these
205 two bottles, formate was the primary electron carrier according to the stoichiometry. This
206 difference in formate generation indicates that *D. vulgaris* was capable of extensively altering the
207 distribution of $H_2$ versus formate production from exogenic pyruvate. By diverting electrons from
208 $H_2$ to formate, pyruvate fermentation avoided the inhibition present with lactate. The formate that
209 accumulated in the liquid became an electron reservoir available for the slower electron-accepting
210 processes associated with Fe(III) (hydr)oxides. The phenomenon was similar to the utilization of
211 propionate as another source of electron reservoir for sulfate and Fe(III) oxide reductions recently
212 observed in a mixed culture [44].

213 **3.2. Enzymatic versus nonenzymatic reductions of Fe(III) (hydr)oxide solids**

214 Pyruvate was much more effective than lactate for Fe(III) (hydr)oxide reduction. According
215 to the mass distribution calculations in Table 2 and Figure 3, over 97% of all three Fe(III)
216 (hydr)oxides were reduced when pyruvate was the electron donor, while lactate led to only ~75%
217 reductions of goethite and ferrihydrite and less than 33% hematite reduction.

218 In all experiments, all 7.4±0.5 mM sulfate was reduced to sulfide, with the potential to
219 nonenzymatically reduce the same amount of each Fe(III) (hydr)oxide; thus, the discrepancy of

reduced Fe from each Fe(III) (hydr)oxide can be attributed to enzymatic reactions. The considerably lower maximum concentrations of soluble $Fe^{2+}$ in the lactate-stimulated bottles (Fig. 1) and mass distribution calculations (Table 2) reveal that enzymatic reduction of Fe(III) (hydr)oxides was much less when lactate was the electron donor, and one of the underlying causes was incomplete lactate fermentation, which resulted in less production of formate and $H_2$.

Recent research [45] discovered that a small portion (>10%) of thiosulfate, besides the dominant $S^0$, were also produced through abiotic ferrihydrite reduction coupled with sulfide oxidation in presence of the sulfur-reducing bacterium *Sulfurospirillum deleyianum*, but the mechanisms remain unknown. In all our experiments, thiosulfate concentrations were below detection limit (>0.1% of total initial sulfate); the selection towards thiosulfate or $S^0$ might be driven by distinct S-cycling metabolisms of different bacteria, and further insightful research is needed to address the phenomenon.

### 3.3. Competition between sulfate and Fe(III) reductions

When lactate was the electron donor, 99% sulfate reduction required less than 2 days in all three bottles. Although a slight amount of Fe(III) (hydr)oxides probably had been enzymatically reduced, soluble $Fe^{2+}$ did not appear before sulfate reduction was complete. When pyruvate was the electron donor, the appearance of $Fe^{2+}$ before completion of sulfate reduction documented Fe(III) (hydr)oxide reduction. Furthermore, sulfate reduction was significantly slowed when Fe(II) accumulated. As a result, *D. vulgaris* required a longer time to reach 99% sulfate reduction coupled with pyvuate than with lactate.

The distinct patterns for the two $e^-$ donors probably resulted from different $e^-$ transfer patterns between lactate and pyruvate. When sulfate was present, the electrons released from lactate fermentation to pyruvate were transferred for sulfate reduction exclusively, while the electrons

from pyruvate fermentation to acetate were proportioned to cytoplasmic sulfate reduction and periplasmic $H_2$/formate formation. With this scenario, sulfate reduction had higher priority than Fe(III) (hydr)oxide reduction when *D. vulgaris* utilized lactate. This scenario is consistent with the proposed model of electron flow proposed by Keller et al [26] for *D. alaskensis* G20.

### 3.4. Fe(III) (hydr)oxide dissolution by citrate

Citrate concentrations were stable during incubations for all the conditions in our *D. vulgaris* tests (Fig. S2). This phenomenon, consistent with what earlier research observed [11, 46-48], further confirmed that *D. vulgaris* is not able to utilize citrate as an electron donor and/or carbon source. Rather, citrate in the matrix functioned as 1) a pH buffer to maintain a favorable pH range (6-8) for *D. vulgaris*, and 2) an iron chelator to prevent iron from precipitation with anions other than sulfide, such as $PO_4^{3-}$, $OH^-$, and $CO_3^{2-}$ [11, 49]. Furthermore, previous research reported the abiotic dissolution of Fe(III) (hydr)oxides by citrate, which enhanced subsequent microbial reduction [50-52]. The proposed mechanism mainly includes 1) the adsorption of citrate on the solid surface through ligand exchange, which not only weakens the surface structure of the larger-sized aggregates, but also stabilization of smaller-sized colloids from further aggregation; and, 2) the fast and slow detachment/dissolution of Fe(III)-citrate from the large aggregates and small colloids, respectively [52, 53]. Overall, the dissolution of Fe(III) enhances its bioavailability towards microbial Fe(III) reduction.

In order to understand the contribution of 19.4 mM citrate in the matrix of all our biotic experiments, we conducted a series of abiotic tests featuring the same concentration of citrate for all three Fe(III) (hydr)oxides and both electron donors at three initial pHs: 6, 7, and 8. These tests followed the incubation procedure of the biotic tests inoculated with *D. vulgaris*. Figure 4 shows the final iron speciation after the 30-day period. During the tests, we observed buildup of

266 significant soluble Fe(III) (from 19% in L+G to 43% in 43% in L+H) only when the initial pH was
267 6. This observation is in accord with previous research reporting faster dissolution under acidic
268 circumstances [50, 52], probably due to that the reaction of citrate adsorption by substituting citrate
269 ions for hydroxide ions was driven and controlled by the initial hydroxide concentration.

270 According to stoichiometry, lactate oxidation coupled with sulfate and Fe(III) reductions
271 consumes protons, resulting in a pH increase, while pyruvate fermentation, in contrast, produces
272 protons and thus decreases the pH. Consistently in our biotic tests, the pH was above 7 in all
273 lactate-stimulated bottles, but was below 7 after a few days in all pyruvate-stimulated bottles, and
274 even reached as low as 6.3 in the P+H bottles (Fig. S3). Thus, in the pyruvate-stimulated bottles,
275 citrate more effectively dissolved Fe(III), and the consequent enhancement of Fe(III)
276 bioavailability, together with the complete utilization of pyruvate via formate, led to
277 distinguishably better Fe(III) reduction (Table 2).

278 **3.5. FeS production and characteristics**

279 When lactate was the electron donor, *D. vulgaris* only reduced 32% of the hematite. As a
280 result, FeS solids produced from hematite were least abundant (0.6 mmole/bottle, 24% of the total
281 iron), compared to goethite (0.9 mmole/bottle, 69% of the total iron) and ferrihydrite (1.5
282 mmole/bottle, 51% of the total iron). EDX analyses (Fig. 5) further confirm this trend: Solids
283 from the H-L bottles had a lower S:Fe signal ratio than solids from other two bottles.

284 When pyruvate was the electron donor, *D. vulgaris* reduced 97% of the Fe(III) (hydr)oxides
285 and consequently produced more FeS than with lactate (Table 2; Fig. 3). This difference was
286 clearly confirmed by the high S:Fe signal ratio in the EDX spectrum of the solids from the G+P
287 bottles (Fig. 5). For the other two bottles, however, the S:Fe signal ratio was lower (Fig. 5) because
288 more soluble $Fe^{2+}$ precipitated as vivianite [$Fe_3(PO_4)_2 \cdot 8(H_2O)$], which is discussed below.

Existence of FeS at the solid surface was confirmed in the XPS spectra by the special tiny humps on the Fe 2p2/3 peak at 707.5-707.6 eV representing the Fe(II)-S bond [54, 55], but only explicit in the samples from the pyruvate experiments (Fig. 6). The apparently higher FeS production with pyruvate probably can be attributed to the stronger XPS signals from the FeS produced with lactate.

Crystalline mackinawite was clearly present as a solid product from the two ferrihydrite-containing bottles (F+L and F+P), but was difficult to recognize in the solid products from other bottles by XRD (Fig. 7). TEM imaging did not allow us to examine lattice fringes for most of the solid samples on <20-nm length scales due to severe damage to sulfur and organic matter (Fig. S4) due to the high energy of the electron beams for magnifications over 140,000X [56, 57]. We were able to observe lattice fringes only in a limited area of the solid sample from the H+L and G+P bottles (Fig. S5).

In the H+L samples, higher average spacing ($5.3 \pm 0.1$Å) corresponded to *d*-spacing of (001) planes of mackinawite, while smaller average spacing ($3.3 \pm 0.5$Å) corresponded to *d*-spacing of (101) planes of mackinawite [58-60]. The thickness of individual crystals calculated by multiplying the number of (001) fringes by the average *d*-spacing was 4.8 nm. This value is very close to the thickness of mackinawite from the F+L bottles (4.9 nm; Table 1) calculated from Eqn. 2 on basis of the XRD data.

In the G+P samples, TEM detected lattice fringes at two nearby locations (Fig. S5). In the brighter area on the left, the average *d*-spacing value of $3.0 \pm 0.5$Å may indicate the presence of mackinawite. In the darker area on the right, the average *d*-spacing values ($4.2 \pm 0.2$Å and $2.7 \pm 0.1$Å) were close to the *d*-spacing values of common goethite (4.18Å and 2.69 Å) [31].

The detectable FeS solids were either in amorphous states or nano-crystalline mackinawite, suggesting a retarded crystallization process, probably due to depletion of sulfide, as reported by previous research [24, 61, 62].

### 3.6. Presence of elemental Sulfur

Elemental sulfur, produced via chemical Fe(III) reduction by sulfide, was expected to be present in the final solids from all the bottles. The chemical analyses (Table 1) and the mass-distribution calculations (Table 2) reveal that $S^0$ accounted for a significant fraction of the original sulfate-S in the solids from the G+L and G+P bottles (37% and 36%, respectively), but were absent in other bottles. The routine analyses of sulfide and S °in ferrihydrite bottles (Fig. S6) revealed $S^0$ accumulation followed by its consumption. This phenomenon is consistent with previous research [63] that demonstrated slow $S^0$ reduction by the pure cytochrome $c_3$ extracted from *Desulfovibrio* species. In addition, although *D. vulgaris* did not grow with elemental sulfur as a respiratory electron acceptor, sulfide was formed from elemental sulfur to a limited extent [64, 65]. The limited and slow process allowed us to observe the presence of $S^0$ in the solids from only the goethite test, which had a shorter duration than the hematite and ferrihydrite tests. Overall, the appearance of $S^0$ further confirmed the chemical reduction of Fe(III) (hydr)oxides by sulfide.

Raman spectra of G+L and G+P solids (Fig. 8) show three prominent peaks at 154, 219, and 473 $cm^{-1}$ corresponding to elemental sulfur ($S_8^0$) [66]. XRD did not detect crystalline $S^0$ in G+L and G+P solids, probably due to its presence in an amorphous form. Single $S^0$ signal was not detected in any area by EDX either, due to its rapid melting and evaporation (Fig. S4) caused by the high energy of the electron beams for higher magnifications [56, 57].

### 3.7. Calcium-phosphate precipitation

Phosphate uptake into the *D. vulgaris* biomass was minimal. According to stoichiometry [67], microbial growth through respiration of 7 mole sulfate and/or Fe(III) requires <0.1 mM phosphate; this small change was less than the detection limit of IC. Thus, detectable change of phosphate concentration in the liquid matrix mainly resulted from precipitation with metals.

In our tests, when lactate was the electron donor, the phosphate concentration in the medium was almost constant (2.6±0.3 mM) through the incubation period in the G+L bottle, but gradually dropped by 0.9±0.1 mM after day 8 and day 6 in the H+L and F+L bottles, respectively. Phosphate loss corresponded to pH higher than 7.4 (Fig. S3). In addition, EDX detected strong signals of calcium (Ca) and phosphorus (P), as well as weaker signals of magnesium (Mg), in all three samples. The presence of P corresponded with phosphate loss in the H+L and F+L bottles. Further EDX scanning in selected areas (Fig. S7) reveals that Ca, Mg, and P were mostly at the edges, but not in the center of the aggregate.

Previous research [68] reported precipitation of $Ca_5(PO_4)_3OH$ at slightly alkaline pH values (normally higher than 7.4). The final pHs in all lactate-stimulated bottles were all above 7.4 (Table 1; Fig. S3); this allowed calcium and phosphate precipitation, most likely in the form of $Ca_5(PO_4)_3OH$. In contrast, the final weakly acidic or neutral pH conditions in all three pyruvate-stimulated bottles did not allow $Ca_5(PO_4)_3OH$ precipitation.

XRD scanning did not detect any Ca- or P-associated crystallites in lactate-stimulated bottles (Fig. 7), indicating that the precipitates were still amorphous, in line with the proposed inhibitive effect of Mg on $Ca_5(PO4)_3OH$ crystallization by substituting in and disrupting the calcium-phosphate crystal lattice or by adsorbing onto the growing calcium phosphate crystals [69, 70].

Though Ca-Mg-P precipitation was an independent chemical process that did not affect Fe(III) and sulfate reduction, its aggregation on the surface of FeS solids may affect the reactivity of FeS.

### 3.8. Vivianite formation

When pyruvate was the electron donor, the greater accumulation of soluble $Fe^{2+}$ from hematite and ferrihydrite was followed by major concentration decreases: 1.3 mM and 0.8 mM, concomitant with 2.0 mM (91%) and 1.0 mM (72%) phosphate loss, respectively. XRD analysis (Fig. 7) confirmed the formation of well-crystallized vivianite, and this explains the high O signals in the EDX spectra (Fig. 5). EDX scanning in selected areas revealed that vivianite had aggregated into large crystals taking a slab (Fig. S8) or a bullet (Fig. S9) shape from the H+P and F+P bottles, respectively.

Vivianite is rapidly formed when free ferrous and phosphate ions are present at near-neutral pH [71, 72]. Previous research [73-75] revealed that free sulfide inhibited vivianite formation, but FeS precipitation and Fe(III) (hydr)oxide reductions scavenged sulfide and thus cleared the inhibitive effect in all our experiments. Completion of pyruvate fermentation led to a build-up of soluble $Fe^{2+}$ high enough (5.5 and 4.6 mM in the H-P and F-P bottles, respectively) to exceed the equilibrium threshold determined by the vivianite solubility product and resulted in precipitation. This is confirmed by the modeling calculation presented in Figure S10.

## 4. Conclusion

In this study, we observed that the distinctly different patterns of electron donor utilization by *D. vulgaris* significantly affected the amount and type of FeS solids through Fe(III) and sulfate reduction, along with the generation of other solids. When lactate was the electron donor, $H_2$ was the primary electron carrier available for respiring $SO_4^{2-}$ and Fe(III). Lactate fermentation was inhibited once sulfate reduction was completed, due to a small accumulation of $H_2$. Lacking electrons for further enzymatic reductions of Fe(III) (hydr)oxide, *D. vulgaris* could not reduce all

the Fe(III) (hydr)oxides and, thus, produced limited amounts of FeS when lactate was the fermentable substrate. In contrast, pyruvate enhanced the production of nano-particulate FeS due to 1) electron diversion from inhibitive $H_2$ to non-inhibitive formate to realize its complete utilization, and 2) more proton release during its fermentation to facilitate Fe(III) (hydr)oxide dissolution by citrate as well as to prevent Ca-$PO_4$ precipitation. The only drawback is accumulation of soluble $Fe^{2+}$ from more hematite or ferrihydrite reduction – due to complete pyruvate fermentation – that led to precipitation of crystalline vivianite [$Fe_3(PO_4)_2 \cdot 8(H_2O)$]. In summary, pyruvate is a better electron donor and carbon source than lactate for producing large amounts of biogenic mackinawite for potential applications in uranium remediation, but the concentrations of calcium and phosphate need to be controlled to avoid precipitation of other minerals.

## Acknowledgements

We express gratitude to the Office of Science, U.S. Department of Energy, Grant No. DE-FG02-09ER64803, for supporting this research. We acknowledge Tara Clancy and Giridhar Upadhyaya at University of Michigan for assistence in establishing the solid washing protocol and growth media conditions for the biogenic production of mackinawite. We also acknowledge Yuqiang Bi at University of Michigan in analyzing a part of samples. We gratefully acknowledge the use of facilities supervised by Thomas Groy at the Department of Chemistry and biochemistry, and by Karl Weiss, Timothy Karcher, and Emmanuel Soignard in the LeRoy Eyring Center for Solid State Science, all at Arizona State University.

## References


1. V. K. Sharma, J. Filip, R. Zboril and R. S. Varma, *Chemical Society Reviews*, 2015.
2. M. A. A. Schoonen, in *Sulfur Biogeochemistry: Past and Present*, eds. J. P. Amend, K. J. Edwards and T. W. Lyons, Geological Society of America, Boulder, CO, USA, 2004, pp. 117-134.
3. D. Rickard and J. W. Morse, *Marine Chemistry*, 2005, **97**, 141-197.
4. M. Maurer and B. E. Rittmann, *Biodegradation*, 2004, **15**, 405-417.
5. S. P. Hyun, J. A. Davis, K. Sun and K. F. Hayes, *Environmental Science & Technology*, 2012, **46**, 3369-3376.
6. H. Veeramani, A. C. Scheinost, N. Monsegue, N. P. Qafoku, R. Kukkadapu, M. Newville, A. Lanzirotti, A. Pruden, M. Murayama and M. F. Hochella, *Environmental Science & Technology*, 2013, **47**, 2361-2369.
7. A. Abdelouas, W. Lutze and H. E. Nuttall, *Journal of Contaminant Hydrology*, 1999, **36**, 353-375.
8. H. S. Moon, J. Komlos and P. R. Jaffe, *Journal of Contaminant Hydrology*, 2009, **105**, 18-27.
9. L. N. Moyes, R. H. Parkman, J. M. Charnock, D. J. Vaughan, F. R. Livens, C. R. Hughes and A. Braithwaite, *Environmental Science & Technology*, 2000, **34**, 1062-1068.
10. Y. Bi, S. Hyun, R. K. Kukkadapu and K. F. Hayes, *Geochimica Et Cosmochimica Acta*, 2013, **102**, 175-190.
11. C. Zhou, R. Vannela, K. F. Hayes and B. E. Rittmann, *Journal of Hazardous Materials*, 2014, **272**, 28-35.
12. K. A. Weber, L. A. Achenbach and J. D. Coates, *Nature Reviews Microbiology*, 2006, **4**, 752-764.
13. B. Yan, B. A. Wrenn, S. Basak, P. Biswas and D. E. Giammar, *Environmental Science & Technology*, 2008, **42**, 6526-6531.
14. J. M. Zachara, J. K. Fredrickson, S. C. Smith and P. L. Gassman, *Geochimica Et Cosmochimica Acta*, 2001, **65**, 75-93.
15. R. K. Sani, B. M. Peyton, J. E. Amonette and G. G. Geesey, *Geochimica Et Cosmochimica Acta*, 2004, **68**, 2639-2648.
16. T. M. Flynn, E. J. O'Loughlin, B. Mishra, T. J. DiChristina and K. M. Kemner, *Science*, 2014, **344**, 1039-1042.
17. D. R. Lovley, J. D. Coates, E. L. BluntHarris, E. J. P. Phillips and J. C. Woodward, *Nature*, 1996, **382**, 445-448.
18. G. Reguera, K. D. McCarthy, T. Mehta, J. S. Nicoll, M. T. Tuominen and D. R. Lovley, *Nature*, 2005, **435**, 1098-1101.
19. C. E. Turick, L. S. Tisa and F. Caccavo, *Applied and Environmental Microbiology*, 2002, **68**, 2436-2444.
20. M. D. Afonso and W. Stumm, *Langmuir*, 1992, **8**, 1671-1675.
21. S. W. Poulton, M. D. Krom and R. Raiswell, *Geochimica Et Cosmochimica Acta*, 2004, **68**, 3703-3715.
22. S. W. Poulton, *Chemical Geology*, 2003, **202**, 79-94.
23. Y. L. Li, H. Vali, J. Yang, T. J. Phelps and C. L. Zhang, *Geomicrobiology Journal*, 2006, **23**, 103-117.
24. R. B. Herbert, S. G. Benner, A. R. Pratt and D. W. Blowes, *Chemical Geology*, 1998, **144**,

87-97.
25. J. P. Gramp, J. M. Bigham, F. S. Jones and O. H. Tuovinen, *Journal of Hazardous Materials*, 2010, **175**, 1062-1067.
26. K. L. Keller, B. J. Rapp-Giles, E. S. Semkiw, I. Porat, S. D. Brown and J. D. Wall, *Applied and Environmental Microbiology*, 2014, **80**, 855-868.
27. F. O. Morais-Silva, C. I. Santos, R. Rodrigues, I. A. C. Pereira and C. Rodrigues-Pousada, *Journal of Bacteriology*, 2013, **195**, 4753-4760.
28. J. F. Heidelberg, R. Seshadri, S. A. Haveman, C. L. Hemme, I. T. Paulsen, J. F. Kolonay, J. A. Eisen, N. Ward, B. Methe, L. M. Brinkac, S. C. Daugherty, R. T. Deboy, R. J. Dodson, A. S. Durkin, R. Madupu, W. C. Nelson, S. A. Sullivan, D. Fouts, D. H. Haft, J. Selengut, J. D. Peterson, T. M. Davidsen, N. Zafar, L. W. Zhou, D. Radune, G. Dimitrov, M. Hance, K. Tran, H. Khouri, J. Gill, T. R. Utterback, T. V. Feldblyum, J. D. Wall, G. Voordouw and C. M. Fraser, *Nature Biotechnology*, 2004, **22**, 554-559.
29. G. Voordouw, *Journal of Bacteriology*, 2002, **184**, 5903-5911.
30. B.-E. Jugder, J. Welch, K.-F. Aguey-Zinsou and C. P. Marquis, *RSC Advances*, 2013, **3**, 8142-8159.
31. U. Schwertmann and R. M. Cornell, *Iron oxides in the laboratory*, Verlagsgesellschaft, Weinheim, Germany 1991.
32. D. G. Karamanev, L. N. Nikolov and V. Mamatarkova, *Minerals Engineering*, 2002, **15**, 341-346.
33. G. Z. Li, S. Park, D. W. Kang, R. Krajmalnik-Brown and B. E. Rittmann, *Environmental Science & Technology*, 2011, **45**, 8359-8367.
34. M. M. McGuire and R. J. Hamers, *Environmental Science & Technology*, 2000, **34**, 4651-4655.
35. H. Y. Jeong, J. H. Lee and K. F. Hayes, *Geochimica Et Cosmochimica Acta*, 2008, **72**, 493-505.
36. A. R. Lennie, S. A. T. Redfern, P. F. Schofield and D. J. Vaughan, *Mineralogical Magazine*, 1995, **59**, 677-683.
37. I. P. Pankhania, A. M. Spormann, W. A. Hamilton and R. K. Thauer, *Archives of Microbiology*, 1988, **150**, 26-31.
38. M. Martins and I. A. C. Pereira, *International Journal Of Hydrogen Energy*, 2013, **38**, 12294-12301.
39. D. R. Noguera, G. A. Brusseau, B. E. Rittmann and D. A. Stahl, *Biotechnology and Bioengineering*, 1998, **59**, 732-746.
40. V. J. Orphan, *Current opinion in microbiology*, 2009, **12**, 231-237.
41. C. B. Walker, Z. He, Z. K. Yang, J. A. Ringbauer, Q. He, J. Zhou, G. Voordouw, J. D. Wall, A. P. Arkin and T. C. Hazen, *Journal of Bacteriology*, 2009, **191**, 5793-5801.
42. S. Fukuzaki, N. Nishio, M. Shobayashi and S. Nagai, *Applied and Environmental Microbiology*, 1990, **56**, 719-723.
43. S. M. da Silva, J. Voordouw, C. Leitão, M. Martins, G. Voordouw and I. A. C. Pereira, *Microbiology*, 2013, **159**, 1760-1769.
44. M. J. Kwon, M. I. Boyanov, D. A. Antonopoulos, J. M. Brulc, E. R. Johnston, K. A. Skinner, K. M. Kemner and E. J. O'Loughlin, *Geochimica Et Cosmochimica Acta*, 2014, **129**, 177-190.
45. R. Lohmayer, A. Kappler, T. Lösekann-Behrens and B. Planer-Friedrich, *Applied and Environmental Microbiology*, 2014, **80**, 3141-3149.

46. K. Kobayashi and G. W. Skyring, *The Journal of General and Applied Microbiology*, 1982, **28**, 45-54.
47. G. Muyzer and A. J. Stams, *Nature Reviews Microbiology*, 2008, **6**, 441-454.
48. D. Xu and T. Gu, *International Biodeterioration & Biodegradation*, 2014, **91**, 74-81.
49. S. P. Hyun and K. F. Hayes, *Journal of Environmental Engineering-Asce*, 2009, **135**, 1009-1014.
50. L. Y. Liang, A. Hofmann and B. H. Gu, *Geochimica Et Cosmochimica Acta*, 2000, **64**, 2027-2037.
51. J. Bosch, K. Heister, T. Hofmann and R. U. Meckenstock, *Applied and Environmental Microbiology*, 2010, **76**, 184-189.
52. J. Braunschweig, C. Klier, C. Schroder, M. Handel, J. Bosch, K. U. Totsche and R. U. Meckenstock, *Geochimica Et Cosmochimica Acta*, 2014, **139**, 434-446.
53. G. Furrer and W. Stumm, *Geochimica Et Cosmochimica Acta*, 1986, **50**, 1847-1860.
54. F. Basolo and R. G. Pearson, 1967.
55. C. F. Petre and F. Larachi, *Aiche Journal*, 2007, **53**, 2170-2187.
56. D. A. Young, in *Phase diagrams of the elements*, University of California Press, Berkeley and Los Angeles, CA, USA, 1991, ch. 10, pp. 129-132.
57. B. Meyer, *Chemical Reviews*, 1976, **76**, 367-388.
58. H. Ohfuji and D. Rickard, *Earth and Planetary Science Letters*, 2006, **241**, 227-233.
59. M. Wolthers, S. J. Van der Gaast and D. Rickard, *American Mineralogist*, 2003, **88**, 2007-2015.
60. A. R. Lennie, K. E. R. England and D. J. Vaughan, *American Mineralogist*, 1995, **80**, 960-967.
61. R. T. Wilkin and H. L. Barnes, *Geochimica Et Cosmochimica Acta*, 1996, **60**, 4167-4179.
62. R. T. Wilkin and H. L. Barnes, *Geochimica Et Cosmochimica Acta*, 1997, **61**, 323-339.
63. G. Fauque, D. Herve and J. Legall, *Archives of Microbiology*, 1979, **121**, 261-264.
64. H. Biebl and N. Pfennig, *Archives of Microbiology*, 1977, **112**, 115-117.
65. N. Pfennig and H. Biebl, in *The prokaryotes*, eds. M. P. Starr, H. Stolp, H. G. Truper, A. Balows and H. G. Schlegel, Springer, Berlin, Germany, 1981, vol. 1, pp. 941-947.
66. R. L. Aggarwal, L. W. Farrar and D. L. Polla, *Journal Of Raman Spectroscopy*, 2011, **42**, 461-464.
67. B. E. Rittmann and P. L. McCarty, *Environmental biotechnology: principles and applications*, Tata McGraw-Hill Education, 2012.
68. J. F. Ferguson, D. Jenkins and J. Eastman, *Journal Water Pollution Control Federation*, 1973, **45**, 620-631.
69. J. F. Ferguson and P. L. Mccarty, *Environmental Science & Technology*, 1971, **5**, 534-540.
70. C. S. Martens and R. C. Harriss, *Geochimica Et Cosmochimica Acta*, 1970, **34**, 621-625.
71. H. C. B. Hansen and I. F. Poulsen, *Clays and Clay Minerals*, 1999, **47**, 312-318.
72. A. Zegeye, L. Huguet, M. Abdelmoula, C. Carteret, M. Mullet and F. Jorand, *Geochimica Et Cosmochimica Acta*, 2007, **71**, 5450-5462.
73. J. O. Nriagu, *Geochimica Et Cosmochimica Acta*, 1972, **36**, 459-470.
74. D. Postma, *Journal of Sedimentary Petrology*, 1977, **47**, 1089-1098.
75. G. McGowan and J. Prangnell, *Geoarchaeology-an International Journal*, 2006, **21**, 93-111.

## Tables

**Table 1.** Measured concentrations of substrates, intermediates, and products; measured pH; experimental durations; and crystallite thicknesses of biogenic mackinawite for all iron-source conditions and when lactate or pyruvate was the electron donor.

| | | Sulfate | | $Fe^{2+}$ | Sulfide | $S^0$ | Formate | pH | | Duration* | Mackinawite |
|---|---|---|---|---|---|---|---|---|---|---|---|
| | Electron | *initial* | *final* | *final* | *final* | *final* | *max.* | *initial* | *final* | | thickness |
| Iron source | Donor | (mmole / bottle) | | | | | | (s.u.) | | (day) | (nm) |
| Goethite | Lactate | 1.4 | 0.0 | 0.1 | 0.0 | 0.5 | 0.6 | 7.2 | 7.4 | 6 | - |
| | Pyruvate | 1.5 | 0.2 | 0.3 | 0.0 | 0.5 | 2.1 | 7.1 | 6.5 | 6 | - |
| Hematite | Lactate | 1.2 | 0.0 | 0.2 | 0.0 | 0.0 | 0.2 | 6.9 | 7.6 | 20 | 4.8† |
| | Pyruvate | 1.2 | 0.0 | 0.8 | 0.0 | 0.0 | 9.1 | 7.0 | 6.6 | 20 | - |
| Ferrihydrite | Lactate | 1.3 | 0.0 | 0.7 | 0.0 | 0.0 | 0.1 | 7.1 | 8.0 | 43 | 4.9 ‡ |
| | Pyruvate | 1.6 | 0.0 | 0.7 | 0.0 | 0.0 | 4.2 | 7.1 | 7.0 | 43 | 4.2 ‡ |

* Counted from the day when the bottles were inoculated to the day when the bottles were opened for solid collection.

† Calculated on basis of data from TEM images.

‡ Calculated on basis of data from XRD spectra.

**Table 2.** Mass distributions of iron, sulfur, and solid phases at the end of the experiments using goethite, hematite, or ferrihydrite as the iron-based electron acceptor and lactate or pyruvate as the electron donor.

| Iron source | | Goethite | | Hematite | | Ferrihydrite | |
|---|---|---|---|---|---|---|---|
| Electron donor | | Lactate | Pyruvate | Lactate | Pyruvate | Lactate | Pyruvate |
| **Iron species** | Fe(III) (Hydr)oxide | 20 | 3 | 68 | 3 | 24 | 2 |
| (mole/mole as %)* | Soluble Fe(II) | 11 | 25 | 8 | 28 | 25 | 27 |
| | Soluble Fe(III) | 0 | 0 | 0 | 0 | 0 | 0 |
| | $FeS_{(s)}$ | 69 | 72 | 24 | 45 | 51 | 60 |
| | Vivianite [$Fe_3(PO_4)_2 \cdot 8H_2O_{(s)}$] | 0 | 0 | 0 | 24 | 0 | 11 |
| **Sulfur species** | Sulfate | 0 | 0 | 0 | 0 | 0 | 1 |
| (mole/mole as %)† | Soluble sulfide | 0 | 0 | 0 | 1 | 0 | 0 |
| | $FeS_{(s)}$ | 63 | 64 | 100 | 99 | 100 | 99 |
| | Elemental sulfur [$S°_{(s)}$] | 37 | 36 | 0 | 0 | 0 | 0 |
| **Final Solids** | Fe(III) (Hydr)oxide$_{(s)}$ | 19 | 4 | 66 | 3 | 30 | 2 |
| (g/g as %)‡ | $FeS_{(s)}$ | 67 | 82 | 34 | 57 | 70 | 79 |
| | Elemental sulfur [$S°_{(s)}$] | 14 | 14 | 0 | 0 | 0 | 0 |
| | Vivianite [$Fe_3(PO_4)_2 \cdot 8H_2O_{(s)}$] | 0 | 0 | 0 | 40 | 0 | 19 |

* The ratio for iron species refers to the percentage of the mole concentration of each iron-containing compound at the end of a test out of the total mole concentration of Fe added as Fe(III) (hydr)oxide at the beginning of the test.

† The ratio for sulfide species refers to the percentage of the mole concentration of each sulfur-containing compound at the end of a test out of the total mole concentration of S added as sulfate at the beginning of the test.

‡ The ratio for the final solids refers to the percentage of the mass of each type of minerals out of the total solid mass collected and dried at the end of each test.

## Figures

**Figure 1.** Concentrations of Fe(II), sulfate, phosphate, lactate, acetate, and formate during the growth of *D. vulgaris* with lactate as the electron donor and with goethite ( "L+G"), hematite ("L+H"), or 2-line ferrihydrite ("L+F") as the Fe(III) source. Error bars indicate standard deviations of duplicate experiments.

**Figure 2.** Concentrations of Fe(II), sulfate, phosphate, pyruvate, acetate, and formate during the growth of *D. vulgaris* with pyruvate as the electron donor with goethite ( "P+G"), hematite ("P+H"), or 2-line ferrihydrite ("P+F") as the Fe(III) source. Error bars indicate standard deviations of duplicate experiments.

**Figure 3.** The mass of Fe(III) hydroxide solids initially added (bars on the left side) and the simulated final solid products (bars on the right side) separated from the experiments identified in the graph.

**Figure 4.** The final iron speciation after 30-day abiotic tests with citrate.

**Figure 5.** TEM images (left column) and EDX spectra (right column) of solids from the experiments identified in the TEM image.

**Figure 6.** XPS spectra of synthetic Fe(III) (hydr)oxides and biogenic solids separated from the experiments, all identified in the graph.

**Figure 7.** XRD spectra of synthetic goethite (top lines in G-L and G-P), hematite (top lines in H-L and H-P), 2-line ferrihydrite (top lines in F-L and F-P), and solids (bottom lines) separated from the experiments identified in the graph.

**Figure 8.** Raman spectra of the solids from the G+L and G+P experiments.

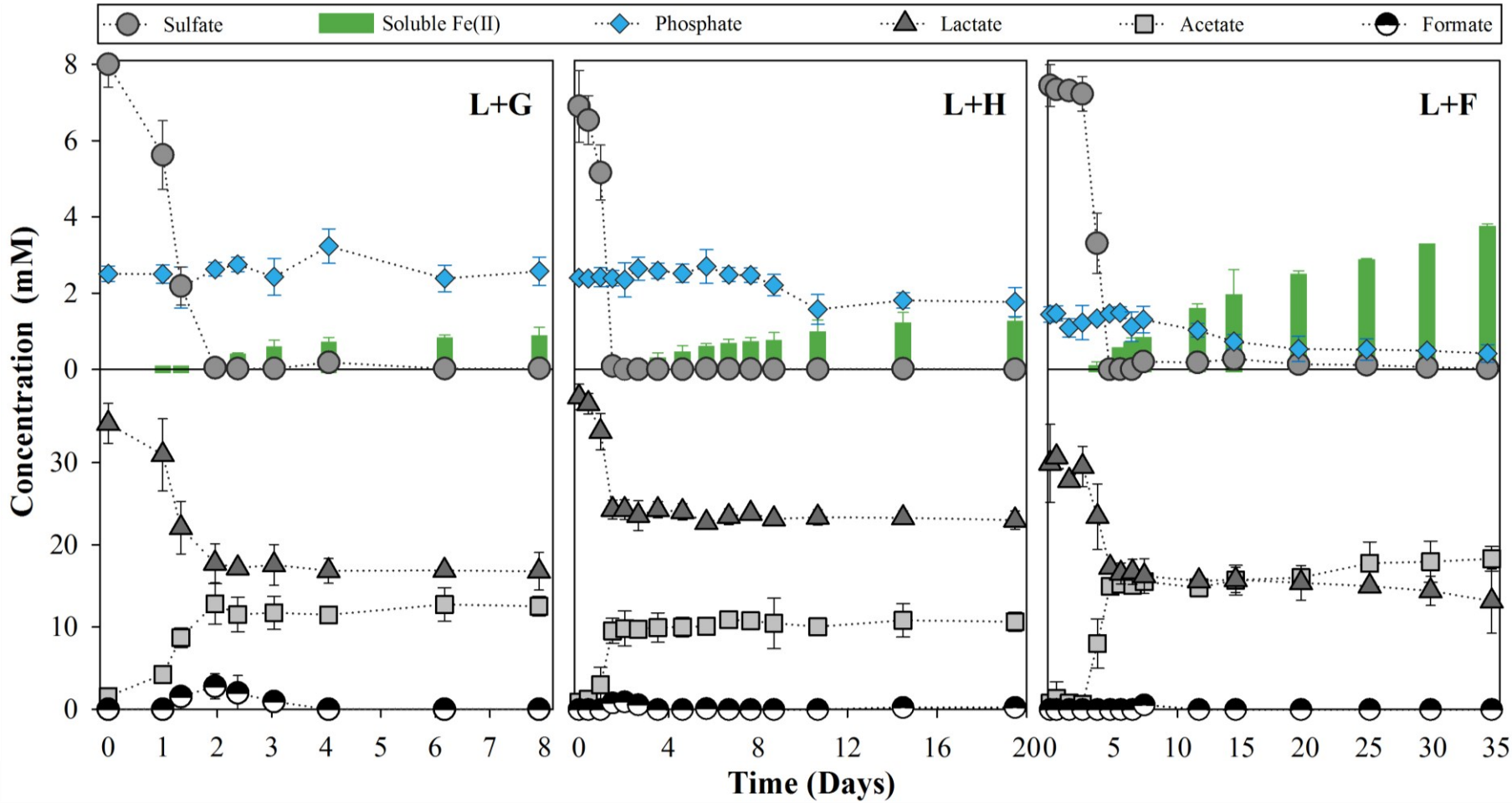


**Figure 1.** Concentrations of Fe(II), sulfate, phosphate, lactate, acetate, and formate during the growth of *D. vulgaris* with lactate as the electron donor and with goethite ( "L+G"), hematite ("L+H"), or 2-line ferrihydrite ("L+F") as the Fe(III) source. Error bars indicate standard deviations of duplicate experiments.

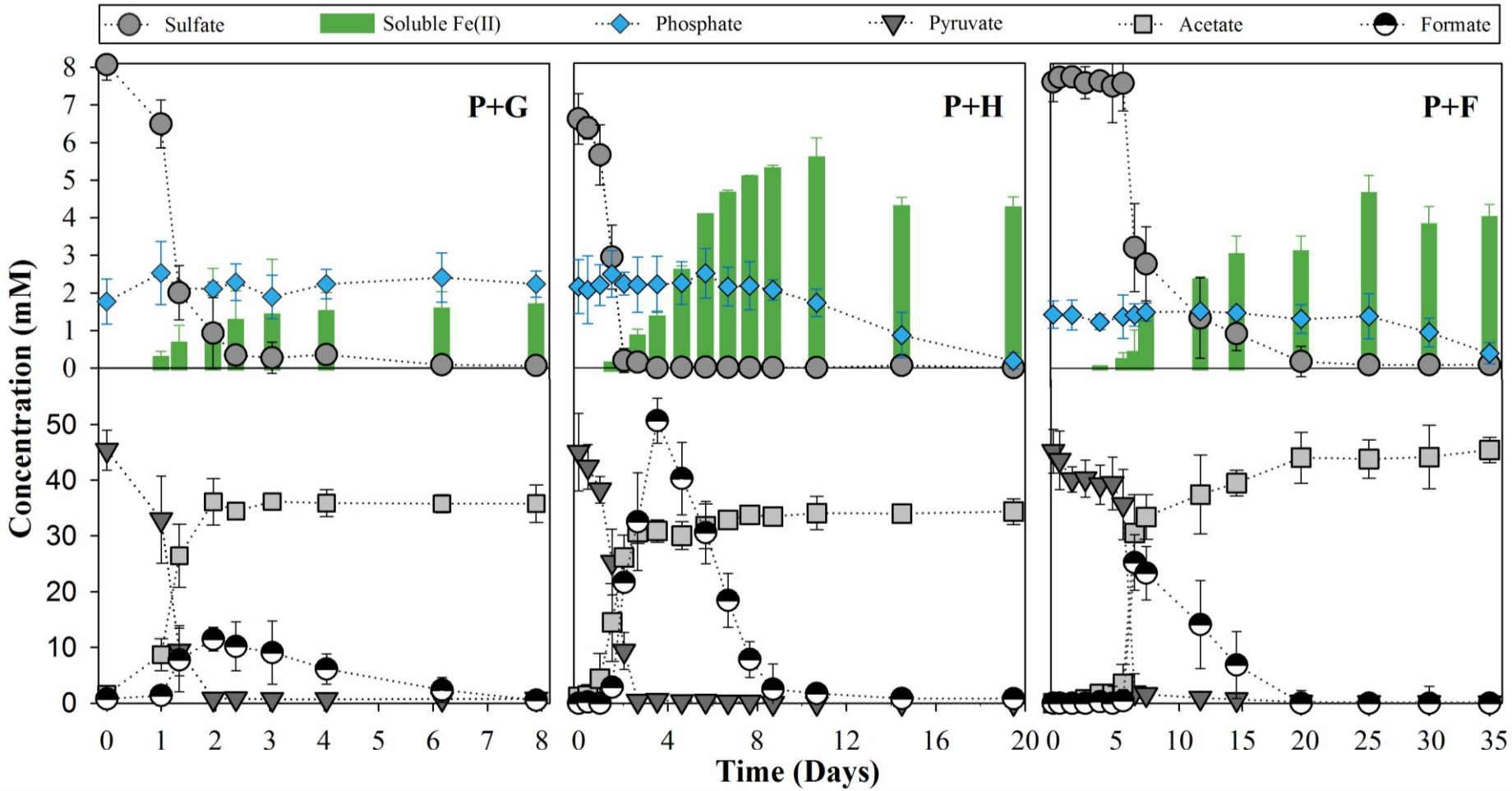


**Figure 2.** Concentrations of Fe(II), sulfate, phosphate, pyruvate, acetate, and formate during the growth of *D. vulgaris* with pyruvate as the electron donor with goethite ("P+G"), hematite ("P+H"), or 2-line ferrihydrite ("P+F") as the Fe(III) source. Error bars indicate standard deviations of duplicate experiments.

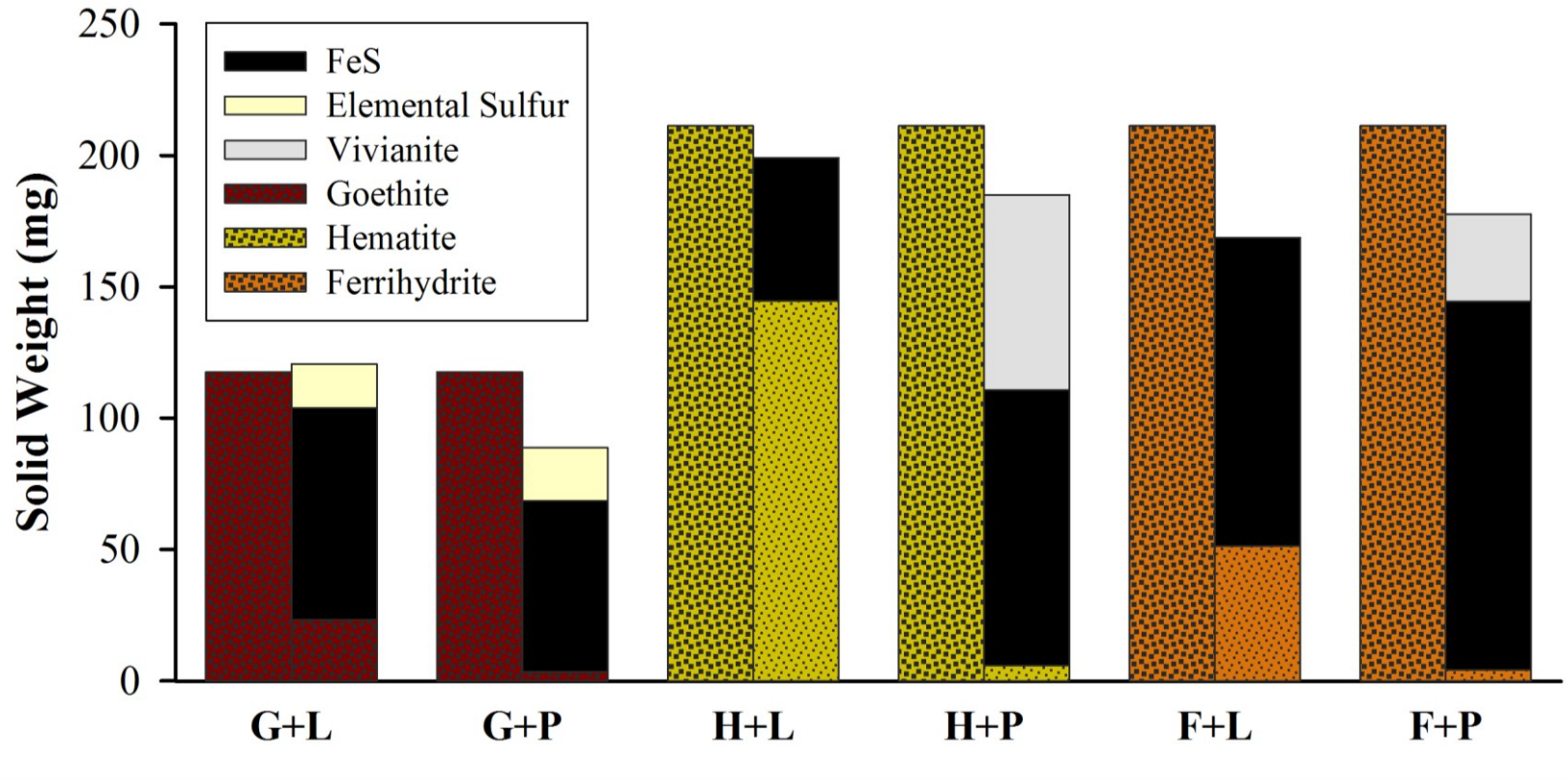


**Figure 3.** The mass of Fe(III) hydroxide solids initially added (bars on the left side) and the simulated final solid products (bars on the right side) separated from the experiments identified in the graph.

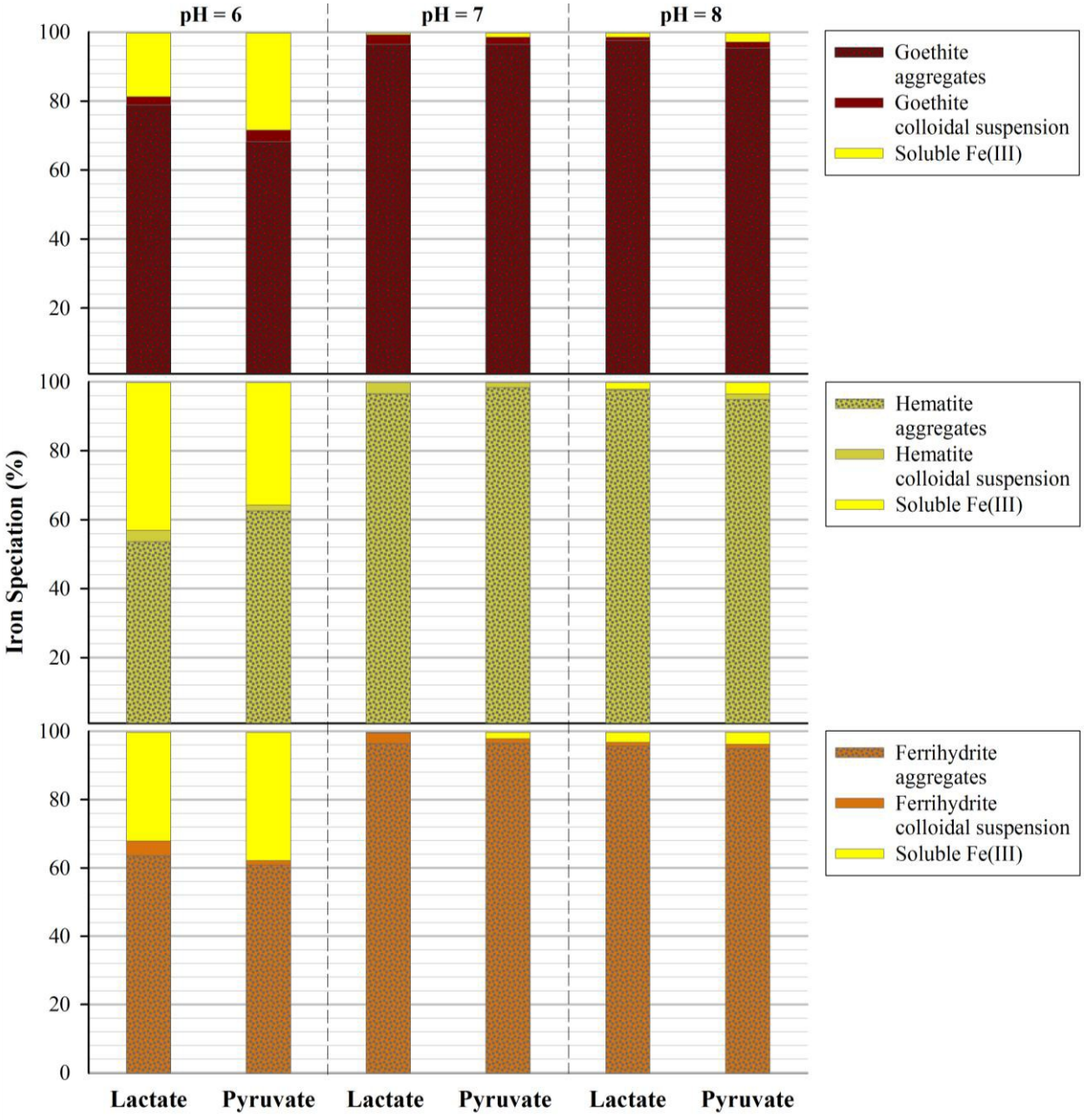


**Figure 4.** The final iron speciation after 30-day abiotic tests with citrate.

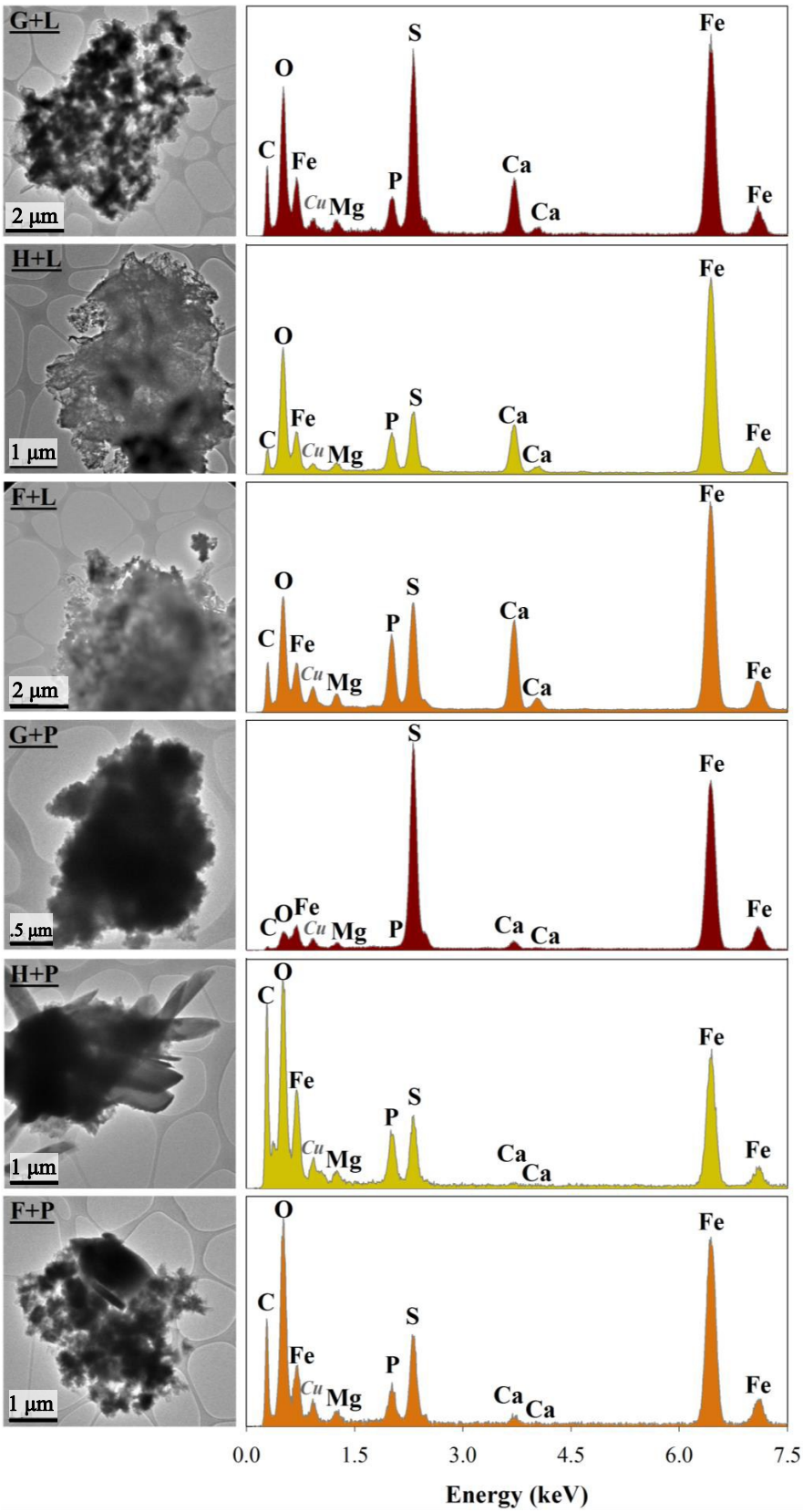


**Figure 5.** TEM images (left column) and EDX spectra (right column) of solids from the experiments identified in the TEM image.

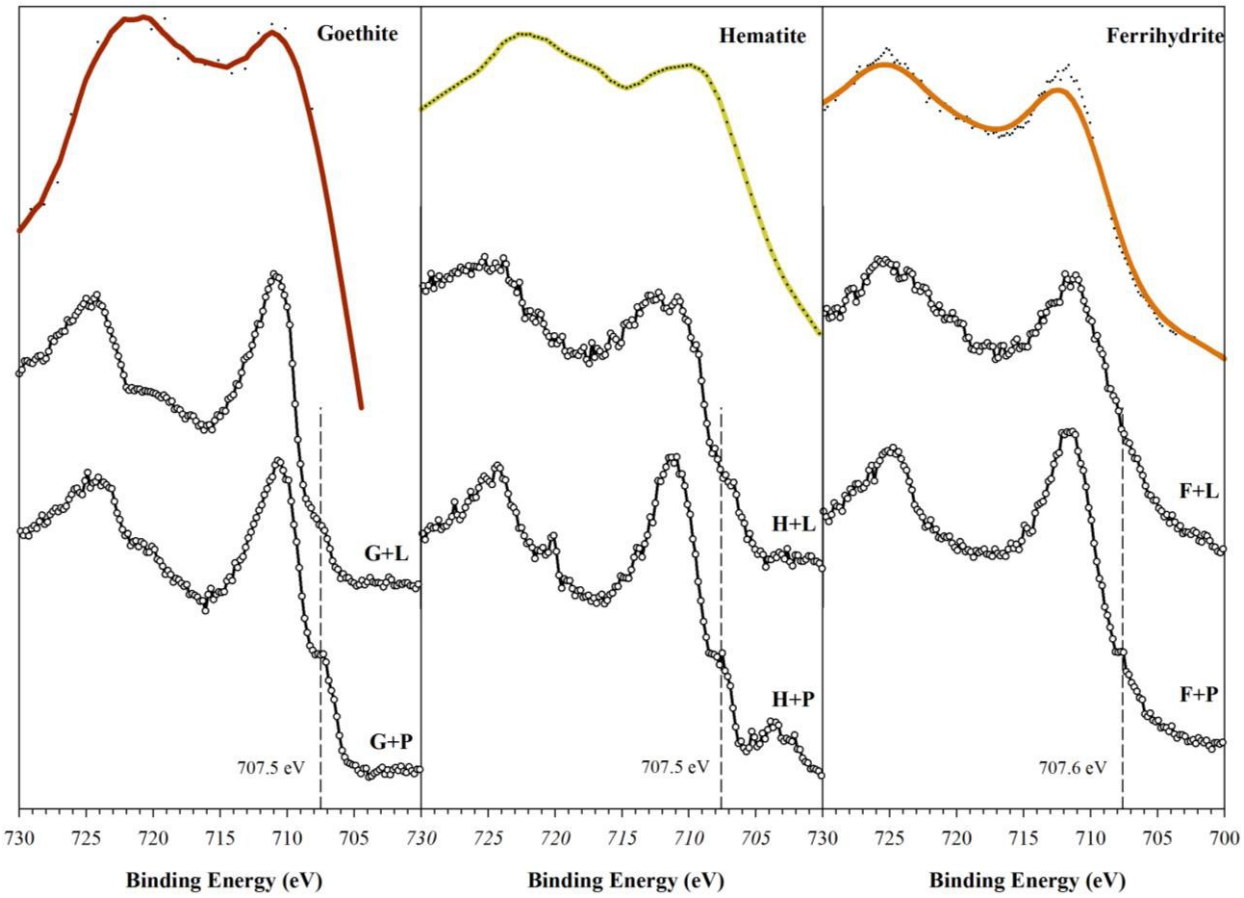


**Figure 6.** XPS spectra of synthetic Fe(III) (hydr)oxides and biogenic solids separated from the experiments, all identified in the graph.

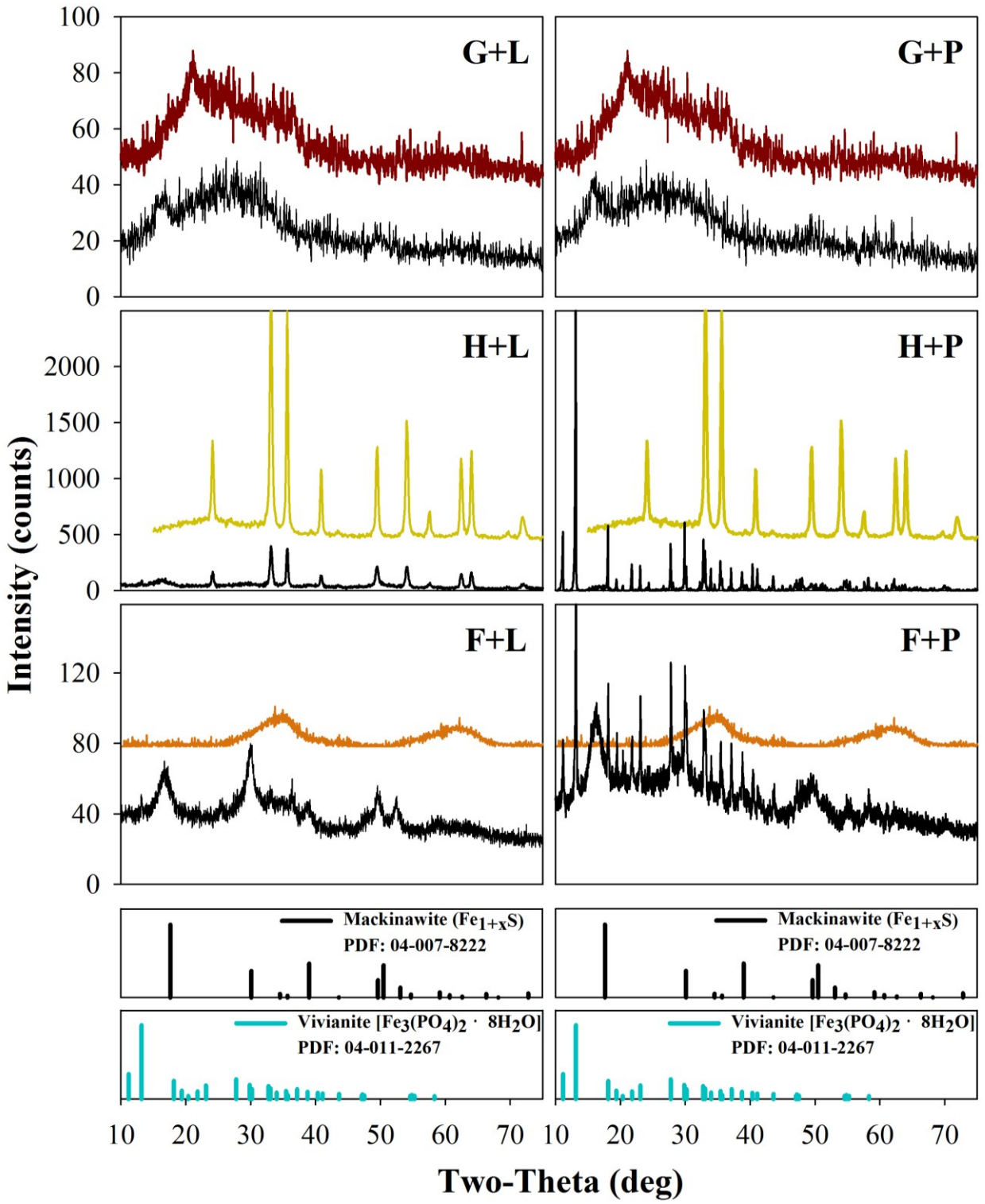


**Figure 7.** XRD spectra of synthetic goethite (top lines in G-L and G-P), hematite (top lines in H-L and H-P), 2-line ferrihydrite (top lines in F-L and F-P), and solids (bottom lines) separated from the experiments identified in the graph.

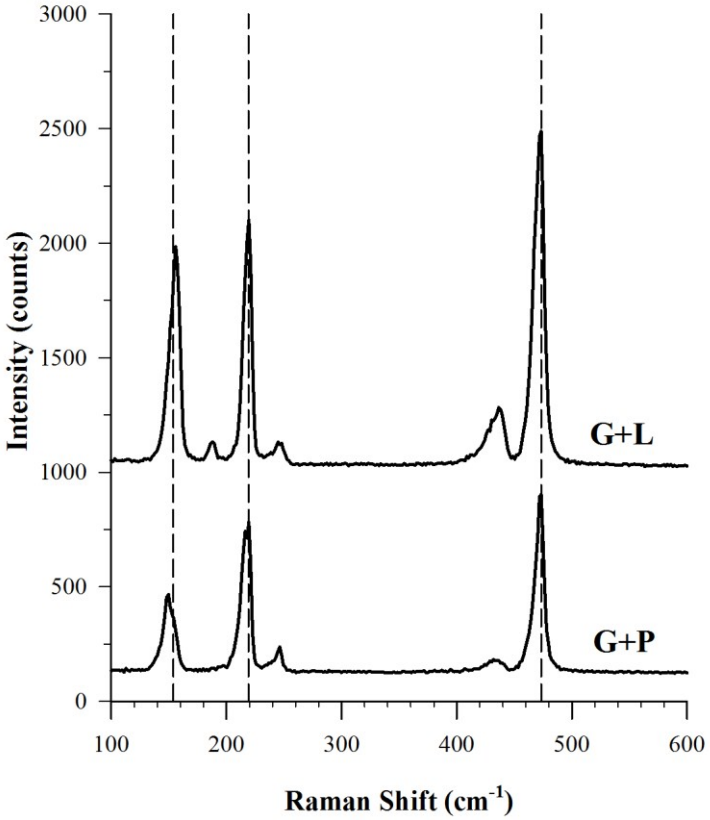


**Figure 8.** Raman spectra of the solids from the G+L and G+P experiments.